Measurement of the branching fraction and time-dependent *CP* asymmetry for $B^0 \to J/\psi\pi^0$ decays

B. Pal,[3,6] A. J. Schwartz,[6] H. Aihara,[83] S. Al Said,[77,35] D. M. Asner,[3] H. Atmacan,[73] V. Aulchenko,[4,62] T. Aushev,[52] R. Ayad,[77] I. Badhrees,[77,34] S. Bahinipati,[19] V. Bansal,[64] P. Behera,[22] C. Beleño,[11] B. Bhuyan,[20] T. Bilka,[5] J. Biswal,[30] A. Bozek,[59] M. Bračko,[46,30] L. Cao,[31] D. Červenkov,[5] V. Chekelian,[47] A. Chen,[56] B. G. Cheon,[13] K. Chilikin,[41] K. Cho,[36] Y. Choi,[75] S. Choudhury,[21] D. Cinabro,[87] S. Cunliffe,[7] N. Dash,[19] S. Di Carlo,[39] Z. Doležal,[5] S. Eidelman,[4,62,41] D. Epifanov,[4,62] J. E. Fast,[64] B. G. Fulsom,[64] R. Garg,[65] V. Gaur,[86] A. Garmash,[4,62] M. Gelb,[31] A. Giri,[21] P. Goldenzweig,[31] B. Golob,[42,30] Y. Guan,[23,15] T. Hara,[15,12] K. Hayasaka,[61] H. Hayashii,[55] T. Higuchi,[32] W.-S. Hou,[58] C.-L. Hsu,[76] K. Inami,[53] A. Ishikawa,[81] R. Itoh,[15,12] M. Iwasaki,[63] Y. Iwasaki,[15] W. W. Jacobs,[23] S. Jia,[2] D. Joffe,[33] T. Julius,[48] G. Karyan,[7] D. Y. Kim,[72] K. T. Kim,[37] S. H. Kim,[13] K. Kinoshita,[6] P. Kodyš,[5] S. Korpar,[46,30] D. Kotchetkov,[14] P. Križan,[42,30] R. Kroeger,[49] P. Krokovny,[4,62] R. Kulasiri,[33] R. Kumar,[68] A. Kuzmin,[4,62] Y.-J. Kwon,[89] K. Lalwani,[45] S. C. Lee,[38] L. K. Li,[24] Y. B. Li,[66] L. Li Gioi,[47] J. Libby,[22] P.-C. Lu,[58] M. Masuda,[82] T. Matsuda,[50] D. Matvienko,[4,62,41] M. Merola,[27,54] K. Miyabayashi,[55] H. Miyata,[61] R. Mizuk,[41,51,52] G. B. Mohanty,[78] T. Mori,[53] E. Nakano,[63] M. Nakao,[15,12] K. J. Nath,[20] Z. Natkaniec,[59] M. Nayak,[87,15] S. Nishida,[15,12] S. Ogawa,[80] H. Ono,[60,61] G. Pakhlova,[41,52] S. Pardi,[27] H. Park,[38] S. Paul,[79] T. K. Pedlar,[44] R. Pestotnik,[30] L. E. Piilonen,[86] V. Popov,[41,52] E. Prencipe,[17] M. V. Purohit,[73] M. Ritter,[43] G. Russo,[27] D. Sahoo,[78] Y. Sakai,[15,12] S. Sandilya,[6] L. Santelj,[15] T. Sanuki,[81] V. Savinov,[67] O. Schneider,[40] G. Schnell,[1,18] J. Schueler,[14] C. Schwanda,[25] Y. Seino,[61] K. Senyo,[88] O. Seon,[53] M. E. Sevior,[48] T.-A. Shibata,[84] F. Simon,[47] A. Sokolov,[26] E. Solovieva,[41,52] M. Starič,[30] M. Sumihama,[10] T. Sumiyoshi,[85] M. Takizawa,[71,16,69] U. Tamponi,[28] K. Tanida,[29] Y. Tao,[8] F. Tenchini,[7] K. Trabelsi,[15,12] M. Uchida,[84] S. Uehara,[15,12] T. Uglov,[41,52] Y. Unno,[13] S. Uno,[15,12] S. E. Vahsen,[14] R. Van Tonder,[31] G. Varner,[14] K. E. Varvell,[76] V. Vorobyev,[4,62,41] B. Wang,[6] C. H. Wang,[57] M.-Z. Wang,[58] P. Wang,[24] X. L. Wang,[9] E. Widmann,[74] E. Won,[37] J. Yelton,[8] J. H. Yin,[24] Z. P. Zhang,[70] V. Zhilich,[4,62] and V. Zhukova[41]

(Belle Collaboration)

[1]*University of the Basque Country UPV/EHU, 48080 Bilbao*
[2]*Beihang University, Beijing 100191*
[3]*Brookhaven National Laboratory, Upton, New York 11973*
[4]*Budker Institute of Nuclear Physics SB RAS, Novosibirsk 630090*
[5]*Faculty of Mathematics and Physics, Charles University, 121 16 Prague*
[6]*University of Cincinnati, Cincinnati, Ohio 45221*
[7]*Deutsches Elektronen–Synchrotron, 22607 Hamburg*
[8]*University of Florida, Gainesville, Florida 32611*
[9]*Key Laboratory of Nuclear Physics and Ion-beam Application (MOE) and Institute of Modern Physics, Fudan University, Shanghai 200443*
[10]*Gifu University, Gifu 501-1193*
[11]*II. Physikalisches Institut, Georg-August-Universität Göttingen, 37073 Göttingen*
[12]*SOKENDAI (The Graduate University for Advanced Studies), Hayama 240-0193*
[13]*Hanyang University, Seoul 133-791*
[14]*University of Hawaii, Honolulu, Hawaii 96822*
[15]*High Energy Accelerator Research Organization (KEK), Tsukuba 305-0801*
[16]*J-PARC Branch, KEK Theory Center, High Energy Accelerator Research Organization (KEK), Tsukuba 305-0801*
[17]*Forschungszentrum Jülich, 52425 Jülich*
[18]*IKERBASQUE, Basque Foundation for Science, 48013 Bilbao*
[19]*Indian Institute of Technology Bhubaneswar, Satya Nagar 751007*
[20]*Indian Institute of Technology Guwahati, Assam 781039*
[21]*Indian Institute of Technology Hyderabad, Telangana 502285*
[22]*Indian Institute of Technology Madras, Chennai 600036*
[23]*Indiana University, Bloomington, Indiana 47408*
[24]*Institute of High Energy Physics, Chinese Academy of Sciences, Beijing 100049*
[25]*Institute of High Energy Physics, Vienna 1050*
[26]*Institute for High Energy Physics, Protvino 142281*
[27]*INFN—Sezione di Napoli, 80126 Napoli*
[28]*INFN—Sezione di Torino, 10125 Torino*

[29]*Advanced Science Research Center, Japan Atomic Energy Agency, Naka 319-1195*
[30]*J. Stefan Institute, 1000 Ljubljana*
[31]*Institut für Experimentelle Teilchenphysik, Karlsruher Institut für Technologie, 76131 Karlsruhe*
[32]*Kavli Institute for the Physics and Mathematics of the Universe (WPI), University of Tokyo, Kashiwa 277-8583*
[33]*Kennesaw State University, Kennesaw, Georgia 30144*
[34]*King Abdulaziz City for Science and Technology, Riyadh 11442*
[35]*Department of Physics, Faculty of Science, King Abdulaziz University, Jeddah 21589*
[36]*Korea Institute of Science and Technology Information, Daejeon 305-806*
[37]*Korea University, Seoul 136-713*
[38]*Kyungpook National University, Daegu 702-701*
[39]*LAL, Université Paris-Sud, CNRS/IN2P3, Université Paris-Saclay, Orsay*
[40]*École Polytechnique Fédérale de Lausanne (EPFL), Lausanne 1015*
[41]*P.N. Lebedev Physical Institute of the Russian Academy of Sciences, Moscow 119991*
[42]*Faculty of Mathematics and Physics, University of Ljubljana, 1000 Ljubljana*
[43]*Ludwig Maximilians University, 80539 Munich*
[44]*Luther College, Decorah, Iowa 52101*
[45]*Malaviya National Institute of Technology Jaipur, Jaipur 302017*
[46]*University of Maribor, 2000 Maribor*
[47]*Max-Planck-Institut für Physik, 80805 München*
[48]*School of Physics, University of Melbourne, Victoria 3010*
[49]*University of Mississippi, University, Mississippi 38677*
[50]*University of Miyazaki, Miyazaki 889-2192*
[51]*Moscow Physical Engineering Institute, Moscow 115409*
[52]*Moscow Institute of Physics and Technology, Moscow Region 141700*
[53]*Graduate School of Science, Nagoya University, Nagoya 464-8602*
[54]*Università di Napoli Federico II, 80055 Napoli*
[55]*Nara Women's University, Nara 630-8506*
[56]*National Central University, Chung-li 32054*
[57]*National United University, Miao Li 36003*
[58]*Department of Physics, National Taiwan University, Taipei 10617*
[59]*H. Niewodniczanski Institute of Nuclear Physics, Krakow 31-342*
[60]*Nippon Dental University, Niigata 951-8580*
[61]*Niigata University, Niigata 950-2181*
[62]*Novosibirsk State University, Novosibirsk 630090*
[63]*Osaka City University, Osaka 558-8585*
[64]*Pacific Northwest National Laboratory, Richland, Washington 99352*
[65]*Panjab University, Chandigarh 160014*
[66]*Peking University, Beijing 100871*
[67]*University of Pittsburgh, Pittsburgh, Pennsylvania 15260*
[68]*Punjab Agricultural University, Ludhiana 141004*
[69]*Theoretical Research Division, Nishina Center, RIKEN, Saitama 351-0198*
[70]*University of Science and Technology of China, Hefei 230026*
[71]*Showa Pharmaceutical University, Tokyo 194-8543*
[72]*Soongsil University, Seoul 156-743*
[73]*University of South Carolina, Columbia, South Carolina 29208*
[74]*Stefan Meyer Institute for Subatomic Physics, Vienna 1090*
[75]*Sungkyunkwan University, Suwon 440-746*
[76]*School of Physics, University of Sydney, New South Wales 2006*
[77]*Department of Physics, Faculty of Science, University of Tabuk, Tabuk 71451*
[78]*Tata Institute of Fundamental Research, Mumbai 400005*
[79]*Department of Physics, Technische Universität München, 85748 Garching*
[80]*Toho University, Funabashi 274-8510*
[81]*Department of Physics, Tohoku University, Sendai 980-8578*
[82]*Earthquake Research Institute, University of Tokyo, Tokyo 113-0032*
[83]*Department of Physics, University of Tokyo, Tokyo 113-0033*
[84]*Tokyo Institute of Technology, Tokyo 152-8550*
[85]*Tokyo Metropolitan University, Tokyo 192-0397*
[86]*Virginia Polytechnic Institute and State University, Blacksburg, Virginia 24061*
[87]*Wayne State University, Detroit, Michigan 48202*

[88]Yamagata University, Yamagata 990-8560
[89]Yonsei University, Seoul 120-749

(Received 29 September 2018; published 19 December 2018)

We measure the branching fraction and time-dependent CP-violating asymmetry for $B^0 \to J/\psi\pi^0$ decays using a data sample of 711 fb^{-1} collected on the $\Upsilon(4S)$ resonance by the Belle experiment running at the KEKB e^+e^- collider. The branching fraction is measured to be $\mathcal{B}(B^0 \to J/\psi\pi^0) = [1.62 \pm 0.11(\text{stat}) \pm 0.06(\text{syst})] \times 10^{-5}$, which is the most precise measurement to date. The measured CP asymmetry parameters are $\mathcal{S} = -0.59 \pm 0.19(\text{stat}) \pm 0.03(\text{syst})$ and $\mathcal{A} = -0.15 \pm 0.14(\text{stat})\,^{+0.04}_{-0.03}(\text{syst})$. The mixing-induced CP asymmetry ($\mathcal{S}$) differs from the case of no CP violation by 3.0 standard deviations, and the direct CP asymmetry ($\mathcal{A}$) is consistent with zero.

DOI: 10.1103/PhysRevD.98.112008

At the quark level, the decay $B^0 \to J/\psi\pi^0$ proceeds via $b \to c\bar{c}d$ "tree" and "penguin" amplitudes, as shown in Fig. 1. Both amplitudes are suppressed in the Standard Model (the first one is color and Cabibbo suppressed), and thus the branching fraction is small. The tree-level amplitude has the same weak phase as that of the $b \to c\bar{c}s$ amplitude governing, e.g., $B^0 \to J/\psi K^0_S$ decays, while the penguin amplitude has a different weak phase. The former dominates mixing-induced CP violation, while the addition of the latter gives rise to direct CP violation.

In the process $\Upsilon(4S) \to B^0\bar{B}^0$, one of the two B mesons can decay into a CP eigenstate f_{CP} at time t_{CP}, while the other can decay into a flavor-specific state f_{tag} at time t_{tag}. The decay time evolution for the $B \to f_{CP}$ is [1]

$$\mathcal{P}(\Delta t, q) = \frac{e^{-|\Delta t|/\tau_{B^0}}}{4\tau_{B^0}} \times (1 + q[\mathcal{S}\sin(\Delta m_d \Delta t) + \mathcal{A}\cos(\Delta m_d \Delta t)]), \quad (1)$$

where $\Delta t = t_{CP} - t_{\text{tag}}$ is the difference in proper decay times between the two B mesons; $q = +1(-1)$ for signal $\bar{B}^0(B^0)$ decays; Δm_d is the mass difference between the two mass eigenstates of the $B^0 - \bar{B}^0$ system; and τ_{B^0} is the B^0 lifetime. The parameters $\mathcal{S}$ and $\mathcal{A}$ are CP violating and characterize mixing-induced and direct CP violation, respectively. In the absence of the penguin amplitude, $\mathcal{A} = 0$ and $\mathcal{S} = -\sin(2\phi_1)$, where $\phi_1 = \arg[-(V^*_{cb}V_{cd})/(V^*_{tb}V_{td})]$. However, this amplitude and any new physics (NP) process having a different weak phase will shift $\mathcal{S}$ and $\mathcal{A}$ from these values. Thus, measuring these parameters provides a way to search for NP. The values of $\mathcal{S}$ and $\mathcal{A}$ measured in $B^0 \to J/\psi\pi^0$ decays can also be used to constrain the small penguin contribution to $B^0 \to J/\psi K^0_S$ decays [2–7]. This small contribution is important as the decay $B^0 \to J/\psi K^0_S$ provides the most precise determination of ϕ_1.

The parameter $\mathcal{S}$ for $B^0 \to J/\psi\pi^0$ has previously been measured by Belle [8] and *BABAR* [9], but the results are not in good agreement. The *BABAR* result lies outside the physically allowed region, but the uncertainties are large. The previous result from Belle was based on 535×10^6 $B\bar{B}$ pairs [8]. Here we update that measurement using the final Belle data set of 772×10^6 $B\bar{B}$ pairs. We also update the $B^0 \to J/\psi\pi^0$ branching fraction, for which our previous measurement used only 32×10^6 $B\bar{B}$ pairs [10]. In addition to more data, the analysis presented here also uses improved tracking and photon reconstruction.

The Belle detector is a large-solid-angle magnetic spectrometer consisting of a silicon vertex detector (SVD), a 50-layer central drift chamber (CDC), an array of aerogel threshold Cherenkov counters, a barrel-like arrangement of time-of-flight scintillation counters, and an electromagnetic calorimeter (ECL) comprising CsI(Tl) crystals. These detector components are located inside a superconducting solenoid coil that provides a 1.5 T magnetic field. An iron flux-return (KLM) located outside the coil is instrumented to detect K^0_L mesons and to identify muons. Two inner detector configurations were used: a 2.0 cm radius beampipe and a three-layer SVD were used for the first 152×10^6 $B\bar{B}$ pairs of data, while a 1.5 cm radius beampipe, a four-layer SVD, and a small-cell inner drift chamber were used for the remaining 620×10^6 $B\bar{B}$

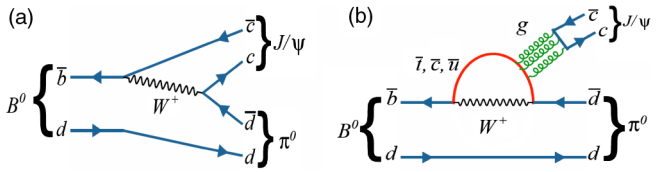

FIG. 1. (a) Tree and (b) penguin amplitudes for the decay $B^0 \to J/\psi\pi^0$.

pairs of data. The detector is described in detail in Ref. [11]. Event selection requirements are optimized using Monte Carlo (MC) simulation. MC events are generated using EvtGen [12], and the detector response is modeled using Geant3 [13]. Final-state radiation is taken into account using the Photos package [14].

The $\Upsilon(4S)$ is produced with a Lorentz boost of $\beta\gamma = 0.425$ along the $+z$ axis, which is defined as antiparallel to the e^+ beam direction. Since the B^0 and $\bar{B}^0$ mesons are approximately at rest in the $\Upsilon(4S)$ center-of-mass (CM) system, Δt is determined from the displacement in z between the two B decay vertices: $\Delta t \approx \Delta z/c\beta\gamma$.

The reconstruction of $B^0 \to J/\psi\pi^0$ proceeds by first reconstructing $\pi^0 \to \gamma\gamma$ candidates. An ECL cluster not matched to any track is identified as a photon candidate. Such candidates are required to have an energy greater than 50 MeV in the barrel region and greater than 100 MeV in the end-cap regions, where the barrel region covers the polar angle $32° < \theta < 130°$ and the end-cap regions cover the ranges $12° < \theta < 32°$ and $130° < \theta < 157°$. We require that the $\gamma\gamma$ invariant mass be within 20 MeV/c^2 (about 3.5σ in resolution) of the π^0 mass [15]. To improve the π^0 momentum resolution, we perform a mass-constrained fit and require that the resulting χ^2 be less than 30. This requirement is relatively loose, retaining more than 99% of events.

We subsequently combine π^0 candidates with J/ψ candidates, which are reconstructed in the e^+e^- and $\mu^+\mu^-$ decay channels. All charged tracks are required to have a minimum number of SVD hits: ≥ 2 in the beam direction, and ≥ 1 in the transverse direction. Electron identification is based on the ratio of the ECL cluster energy to the particle momentum as measured in the CDC, as well as the position and shape of the electromagnetic shower in the ECL. In order to account for radiative energy loss in e^+e^- decays, we include up to two bremsstrahlung photons that lie within 50 mrad of each of the reconstructed tracks when calculating the e^+ and e^- four-momenta. Muons are identified by corresponding hit positions and the track penetration depth in the KLM. The reconstructed J/ψ invariant masses $M_{ee(\gamma)}$ and $M_{\mu\mu}$ are required to satisfy $-150\ \text{MeV}/c^2 < M_{ee(\gamma)} - m_{J/\psi} < +36\ \text{MeV}/c^2$ and $-60\,\text{MeV}/c^2 < M_{\mu\mu} - m_{J/\psi} < +36\,\text{MeV}/c^2$, where $m_{J/\psi}$ is the nominal J/ψ mass [15]. The asymmetric mass ranges account for the radiative tail, which biases the reconstructed mass towards lower values. For selected J/ψ candidates, vertex- and mass-constrained fits are performed to improve the momentum resolution.

Candidate B^0 mesons are identified using the beam-energy-constrained mass $M_{\rm bc} = (\sqrt{E^2_{\rm beam} - |\vec{p}_B|^2c^2})/c^2$, and the energy difference $\Delta E = E_B - E_{\rm beam}$, where $E_{\rm beam}$ is the beam energy, and E_B and $\vec{p}_B$ are the reconstructed energy and momentum, respectively, of the B^0 candidate. All quantities are evaluated in the CM frame. Events satisfying $M_{\rm bc} > 5.24\ \text{GeV}/c^2$ and $-0.20\ \text{GeV} < \Delta E < 0.10\ \text{GeV}$ are retained for further analysis. To calculate the signal yield, we define a smaller signal region: $5.27\ \text{GeV}/c^2 < M_{\rm bc} < 5.29\ \text{GeV}/c^2$ and $-0.10\ \text{GeV} < \Delta E < 0.05\ \text{GeV}$. In order to suppress "continuum" background arising from light quark production ($e^+e^- \to q\bar{q}$, $q = u, d, s, c$), we require that the event shape variable R_2, which is the ratio of the second to zeroth Fox-Wolfram moments [16], satisfies $R_2 < 0.4$.

After applying all selection criteria, 2.9% of events have multiple B^0 candidates in the signal region. For these events, we retain the candidate having the smallest sum of χ^2 values obtained from the $\pi^0 \to \gamma\gamma$ mass-constrained fit and the $J/\psi \to \ell^+\ell^-$ vertex- and mass-constrained fit. According to MC simulations, this criterion selects the correct B^0 candidate in 74% of multiple-candidate events.

We tag (identify) the flavor of the accompanying B meson using inclusive properties of particles not associated with the signal $B^0 \to J/\psi\pi^0$ decay. The algorithm for flavor tagging is described in Ref. [17]. Two parameters, q and r, are used to represent the tagging information. The former is the implied flavor of the signal B decays as used in Eq. (1). The latter is an event-by-event MC-determined quality factor that ranges from $r = 0$ for no flavor discrimination to $r = 1$ for unambiguous flavor assignment. It is used for sorting candidate events into seven r ranges. For events having $r > 0.10$, we determine the wrong-tag fractions ω_l ($l = 1, 7$) and their differences $\Delta\omega_l$ between B^0 and $\bar{B}^0$ decays from a control sample of self-tagged semileptonic and hadronic $b \to c$ decays [18,19]. If $r < 0.10$, the wrong tag fraction is set to 0.5.

The vertex position for the $B^0 \to J/\psi\pi^0$ decay is reconstructed using lepton tracks from the J/ψ decays. We perform a vertex fit with a constraint to the interaction point (IP) profile. A vertex position for $f_{\rm tag}$ is obtained using tracks that are not assigned to the $B^0 \to J/\psi\pi^0$ candidate, plus the IP constraint. This constraint allows for reconstruction of an $f_{\rm tag}$ vertex even in cases when only one track candidate satisfies the requirement on SVD hits. The fraction of single-track vertices for $f_{\rm tag}$ is approximately 12%, estimated from MC. To reject events with poorly reconstructed vertices, we require $\sigma_z < 200\ \mu$m and $h < 50$ for multitrack vertices, and $\sigma_z < 500\ \mu$m for single-track vertices, where σ_z is the error on the vertex z coordinate, and h is the χ^2 value calculated in three-dimensional space without using the IP constraint [19]. We retain events in which both the J/ψ and $f_{\rm tag}$ vertices satisfy $|\Delta t| < 70$ ps.

To extract the signal yield, we perform a two-dimensional unbinned maximum likelihood fit to the variables $M_{\rm bc}$ and ΔE. The probability density function (PDF) of signal events consists of two parts: one for candidates that are correctly reconstructed, and one for those incorrectly reconstructed, i.e., at least one daughter

originates from the other (tag-side) B. For the former case, both the $M_{\rm bc}$ and ΔE distributions are modeled with Crystal Ball (CB) functions [20]. For the latter case, the correlated two-dimensional $M_{\rm bc}-\Delta E$ distribution is modeled with a nonparametric PDF [21]. The fraction of incorrectly reconstructed decays (∼10% in the signal region) is taken from MC simulation. The CB parameters that describe the lower tail of the $M_{\rm bc}$ and ΔE distributions are also fixed to MC values.

The remaining background is small and dominated by $B\bar{B}$ events in which one of the B mesons decays into a final state containing a J/ψ. We divide this background into three categories: (a) $B^0 \to J/\psi K^0_S$, (b) $B^0 \to J/\psi K^0_L$, and (c) $B \to J/\psi X$ other than $B^0 \to J/\psi K^0$. We use two-dimensional nonparametric PDFs [21] to model the $M_{\rm bc}-\Delta E$ distributions for all three categories. We fix the background yields to those expected based on MC simulation: 10.8 $J/\psi K^0_S$ events, 10.0 $J/\psi K^0_L$ events, and 17.5 other $J/\psi X$ events in the $M_{\rm bc}-\Delta E$ signal region. The remaining background comes from continuum $q\bar{q}$ events. We model the $M_{\rm bc}$ and ΔE distributions of continuum background with an ARGUS [22] function having its end point fixed to 5.29 GeV/c^2, and a first-order polynomial, respectively. Background coming from $B\bar{B}$ not containing a real J/ψ is negligible. From the fit we obtain 330.2 ± 22.1 signal events and 16.3 ± 3.5 continuum events. The purity of the signal is 86% in the signal region. Projections of the fit are shown in Fig. 2.

The branching fraction is calculated from the formula

$$\mathcal{B}(B^0 \to J/\psi\pi^0) = \frac{Y_{\rm sig}}{\varepsilon \times N_{B\bar{B}} \times \mathcal{B}_{J/\psi} \times \mathcal{B}_{\pi^0}}, \qquad (2)$$

where $Y_{\rm sig}$ is the fitted signal yield; $N_{B\bar{B}} = (772 \pm 11) \times 10^6$ is the number of $B\bar{B}$ events; $\varepsilon = (22.3 \pm 0.1)\%$ is the signal efficiency for e^+e^- and $\mu^+\mu^-$ combined as obtained from MC simulation; $\mathcal{B}_{J/\psi}$ is the sum of $\mathcal{B}(J/\psi \to \mu^+\mu^-)$ and $\mathcal{B}(J/\psi \to e^+e^-)$ [15]; and $\mathcal{B}_{\pi^0}$ is the branching fraction of $\pi^0 \to \gamma\gamma$ [15]. In Eq. (2) we assume equal production of $B^0\bar{B}^0$ and B^+B^- pairs at the $\Upsilon(4S)$ resonance. The result is

$$\mathcal{B}(B^0 \to J/\psi\pi^0) = (1.62 \pm 0.11 \pm 0.06) \times 10^{-5},$$

where the first uncertainty is statistical and the second is systematic.

The systematic uncertainty on $\mathcal{B}(B^0 \to J/\psi\pi^0)$ arises from several sources, as listed in Table I. The uncertainty due to the fixed parameters in the PDF is estimated by varying each parameter individually according to its statistical uncertainty. The resulting changes in the branching fraction are added in quadrature and the result is taken as the systematic uncertainty. The nonparametric shapes are also varied by changing their smoothing, and the associated systematic uncertainty is found to be negligible. We assign a 1.5% systematic uncertainty due to π^0 reconstruction, as determined from a study of $\tau^- \to \pi^-\pi^0\nu_\tau$ decays [23]. The uncertainty due to charged track reconstruction is 0.35% per track, as determined from a study of partially reconstructed $D^{*+} \to D^0\pi^+$, $D^0 \to K^0_S\pi^+\pi^-$ decays. We assign a 2.1% uncertainty due to lepton identification, as obtained from a study of two-photon $\gamma\gamma \to \ell^+\ell^-$ production events.

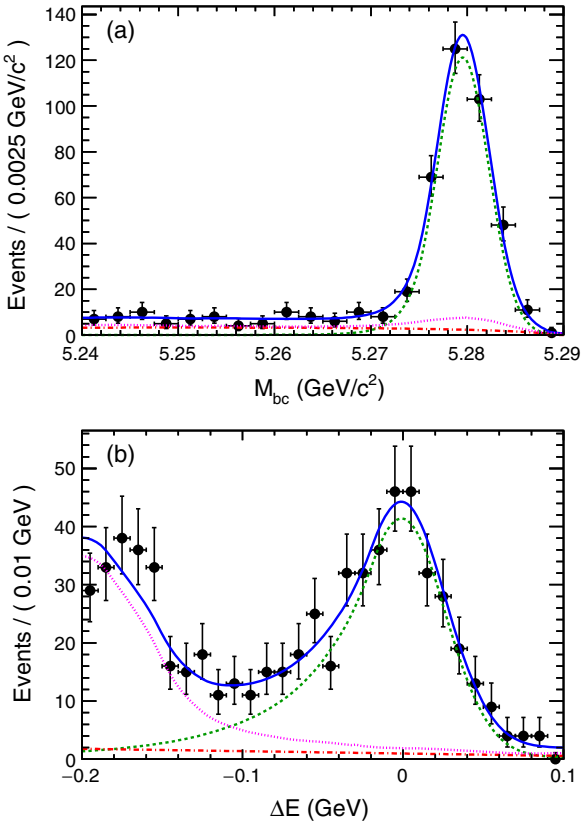

FIG. 2. Projections of the two-dimensional fit: (a) $M_{\rm bc}$ in the ΔE signal region, and (b) ΔE in the $M_{\rm bc}$ signal region. The points are data, the (green) dashed curves show the signal, the (red) dotted-dashed curves show the $q\bar{q}$ background, the (magenta) dotted curves show the $B\bar{B}$ background, and the (blue) solid curves show the total PDF.

TABLE I. Fractional systematic uncertainties for $\mathcal{B}(B^0 \to J/\psi\pi^0)$.

Source	Uncertainty (%)
PDF parametrization	0.1
π^0 reconstruction	1.5
Tracking	0.7
Lepton identification selection	2.1
Incorrectly reconstructed signal events	0.8
$B \to J/\psi(K^0_S, K^0_L, X)$ background	$^{+1.8}_{-2.0}$
MC statistics	0.4
Secondary branching fractions	0.8
Number of $B\bar{B}$ pairs	1.4
Total	$^{+3.7}_{-3.9}$

The uncertainty due to the estimated fraction of incorrectly reconstructed signal events is obtained by varying this fraction by ±100%. As $B \to J/\psi(K^0_S, K^0_L, X)$ decays are well measured, we evaluate the uncertainty due to their estimated amounts by varying them by ±20%. The uncertainty due to the number of $B\bar{B}$ pairs is 1.4%, and the uncertainty on the reconstruction efficiency ε due to the MC sample size is 0.4%. The total systematic uncertainty is obtained by summing all individual contributions in quadrature.

We determine $\mathcal{S}$ and $\mathcal{A}$ by performing an unbinned maximum likelihood fit to the Δt distribution of candidate events in the signal region. The PDF for the signal component, $\mathcal{P}_{\rm sig}(\Delta t; \mathcal{S}, \mathcal{A}, q, \omega_l, \Delta\omega_l)$, is given by Eq. (1) with the parameters τ_{B^0} and Δm_d fixed to the world-average values [24]. We modify this expression to take into account the effect of incorrect flavor assignment, which is parametrized by ω_l and $\Delta\omega_l$. This PDF is then convolved with the decay-time resolution function $R_{\rm sig}(\Delta t)$. The resolution function is itself a convolution of four components: the detector resolutions for $z_{J/\psi\pi^0}$ and $z_{\rm tag}$; the shift of the $z_{\rm tag}$ vertex position due to secondary tracks from charmed particle decays; and the kinematic approximation that the B mesons are at rest in the CM frame [19]. The PDFs for the $B^0 \to J/\psi K^0_S$ and $B^0 \to J/\psi K^0_L$ backgrounds are the same as $\mathcal{P}_{\rm sig}$ but with CP parameters $\mathcal{A}$ and $\mathcal{S}$ fixed to the recent Belle results [19]. The PDF for the $B \to J/\psi X$ background is taken to have the same form as $\mathcal{P}_{\rm sig}$ but with $\mathcal{A}$ and $\mathcal{S}$ set to zero, and with an effective lifetime $\tau_{\rm eff}$ determined from MC simulation. The PDF for continuum background is taken to be the sum of two Gaussian functions whose parameters are obtained by fitting events in the sideband region $5.20\,{\rm GeV}/c^2 < M_{\rm bc} < 5.26\,{\rm GeV}/c^2$ and $0.10\ {\rm GeV} < \Delta E < 0.50\ {\rm GeV}$.

We assign the following likelihood to the ith event:

$$\begin{aligned}\mathcal{P}_i(\Delta t) = (1 - f_{\rm ol}) \int d(\Delta t')[R_{\rm sig}(\Delta t_i - \Delta t') \\ \times (f_{\rm sig}\mathcal{P}_{\rm sig}(\Delta t') + f_{J/\psi K^0_S}\mathcal{P}_{J/\psi K^0_S}(\Delta t') \\ + f_{J/\psi K^0_L}\mathcal{P}_{J/\psi K^0_L}(\Delta t') + f_{J/\psi X}\mathcal{P}_{J/\psi X}(\Delta t')) \\ + f_{q\bar{q}}\mathcal{P}_{q\bar{q}}(\Delta t_i)] + f_{\rm ol}\mathcal{P}_{\rm ol}(\Delta t_i),\end{aligned} \tag{3}$$

where $f_{\rm sig}$, $f_{J/\psi K^0_S}$, $f_{J/\psi K^0_L}$, $f_{J/\psi X}$, and $f_{q\bar{q}}$ are the fractions of the signal, $B^0 \to J/\psi K^0_S$, $B^0 \to J/\psi K^0_L$, $B \to J/\psi X$, and $q\bar{q}$ continuum background, respectively. All fractions depend on the flavor tagging quality r and are functions of ΔE and $M_{\rm bc}$. The term $\mathcal{P}_{\rm ol}(\Delta t)$ is a broad Gaussian function that represents an outlier component with a small fraction $f_{\rm ol} \approx 0.5\%$. The only free parameters in the fit are $\mathcal{S}$ and $\mathcal{A}$; these are determined by maximizing the likelihood $\mathcal{L}(\mathcal{S}, \mathcal{A}) = \prod_i \mathcal{P}_i(\Delta t_i; \mathcal{S}, \mathcal{A})$. Figure 3 shows the fitted Δt distribution and the time-dependent decay rate asymmetry $\mathcal{A}_{CP}$, where $\mathcal{A}_{CP} = (Y^{(q=+1)}_{\rm sig} - Y^{(q=-1)}_{\rm sig})/(Y^{(q=+1)}_{\rm sig} + Y^{(q=-1)}_{\rm sig})$, and $Y^{(q=\pm1)}_{\rm sig}$ is the signal yield with $q = \pm 1$. The results of the fit are

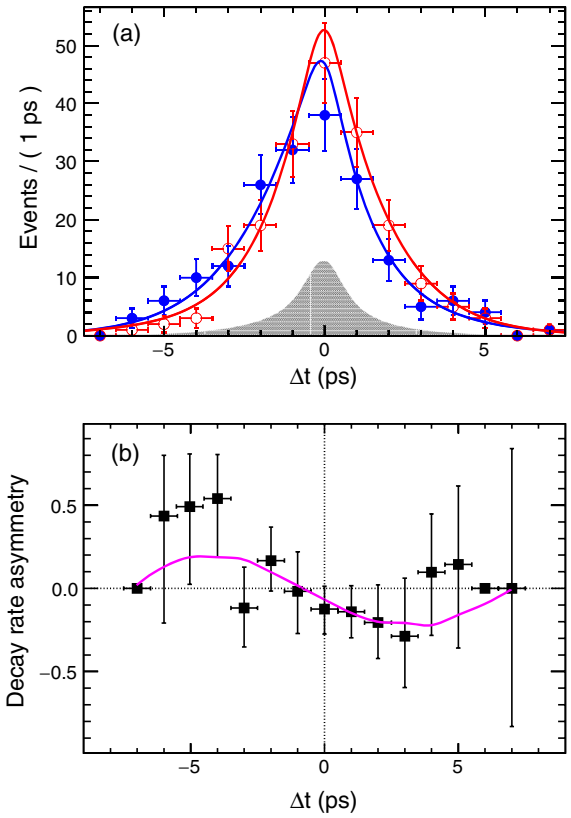

FIG. 3. (a) Distributions of Δt. The (blue) solid and (red) open points represent the $q = +1$ and $q = -1$ events, respectively, and the solid curves show the corresponding fit projections. The gray shaded region represents the sum of all backgrounds. (b) Time-dependent CP asymmetry $\mathcal{A}_{CP}$ (see text).

$$\begin{aligned}\mathcal{S} &= -0.59 \pm 0.19 \pm 0.03 \\ \mathcal{A} &= -0.15 \pm 0.14^{+0.04}_{-0.03},\end{aligned}$$

where the first uncertainty is statistical and the second is systematic. The correlation between $\mathcal{A}$ and $\mathcal{S}$ is −0.005.

The systematic uncertainties for $\mathcal{S}$ and $\mathcal{A}$ are listed in Table II. They are small compared to the corresponding statistical uncertainties. The largest contributions to $\mathcal{S}$ arise from vertex reconstruction and the resolution function. The uncertainty due to the former includes uncertainties in the IP profile, charged track selection, vertex quality selection, and SVD misalignment. We vary each parameter of the resolution function by one standard deviation ($\pm 1\sigma$) and compare the resulting fit result with that of the nominal fit; the difference between the two is taken as the systematic uncertainty. Each physics parameter that is fixed to its world average value [24], e.g., τ_{B^0} and Δm_d, is varied by the corresponding error; the uncertainty is taken to be the

TABLE II. Absolute systematic uncertainties for $\mathcal{S}$ and $\mathcal{A}$.

Source	$\sigma_{\mathcal{S}}$ (%)	$\sigma_{\mathcal{A}}$ (%)
Vertex reconstruction	$^{+2.36}_{-1.75}$	$^{+1.40}_{-2.22}$
Resolution function	$^{+1.43}_{-2.37}$	$^{+1.00}_{-0.91}$
Physics parameters	$^{+0.04}_{-0.03}$	± 0.04
Fit bias	± 0.68	± 0.27
Wrong tag fraction	$^{+0.41}_{-0.20}$	$^{+0.43}_{-0.17}$
$M_{\rm bc}$, ΔE shapes	$^{+0.52}_{-0.45}$	$^{+0.50}_{-0.48}$
Signal and background fraction	$^{+0.71}_{-0.62}$	$^{+0.49}_{-0.72}$
Background Δt shape	$^{+0.20}_{-0.12}$	± 0.10
Tag-side interference	± 0.20	$^{+3.80}_{-0.00}$
Total	$^{+3.02}_{-3.14}$	$^{+4.26}_{-2.57}$

resulting difference with the nominal fit result. The uncertainty due to possible fit bias is evaluated using large ensembles of MC signal events; the differences of the fit results with the MC inputs are assigned as systematic uncertainties. The uncertainties due to ω_l and $\Delta\omega_l$ are estimated by varying these parameters individually by $\pm 1\sigma$. The $M_{\rm bc}$ and ΔE shape parameters, and the fractions of signal and background, are varied to estimate their contributions to the systematic uncertainty. We vary each parameter in $\mathcal{P}_{q\bar{q}}(\Delta t)$ and $\mathcal{P}_{J/\psi X}(\Delta t)$ by $\pm 1\sigma$. For $\mathcal{P}_{J/\psi K^0_S}(\Delta t)$ and $\mathcal{P}_{J/\psi K^0_L}(\Delta t)$, we vary the CP asymmetry parameters by their statistical errors [19]. We include the effect of tag-side interference [25], which introduces a significant contribution to the systematic uncertainty for $\mathcal{A}$. Tag-side interference is caused by interference between the two tree-level amplitudes contributing to $B \to DX$ decays.

In summary, we have measured the branching fraction and time-dependent CP asymmetry for $B^0 \to J/\psi\pi^0$ decays using the full Belle $\Upsilon(4S)$ data set. The results are

$$\mathcal{B} = (1.62 \pm 0.11 \pm 0.06) \times 10^{-5}$$
$$\mathcal{S} = -0.59 \pm 0.19 \pm 0.03$$
$$\mathcal{A} = -0.15 \pm 0.14^{+0.04}_{-0.03},$$

where the first uncertainty is statistical and the second is systematic. The measured value for the branching fraction is the most precise value to date and supersedes the previous measurement [10]. It is consistent with measurements made by other experiments [9,26]. The measured CP asymmetries are consistent with, and supersede, our previous results [8]. The direct CP asymmetry $\mathcal{A}$ is consistent with zero. The mixing-induced CP asymmetry $\mathcal{S}$ differs from zero (i.e., no CP violation) by 3.0σ, and it differs from the *BABAR* result [9] (which is outside the physical region) by 3.2σ. The value is consistent with the value of $\sin 2\phi_1$ measured using $b \to c\bar{c}s$ decays [15]. These results indicate that the penguin and any NP contribution to $B^0 \to J/\psi\pi^0$ are small.

We thank the KEKB group for the excellent operation of the accelerator; the KEK cryogenics group for the efficient operation of the solenoid; the KEK computer group, and the Pacific Northwest National Laboratory (PNNL) Environmental Molecular Sciences Laboratory (EMSL) computing group for strong computing support; and the National Institute of Informatics, and Science Information NETwork 5 (SINET5) for valuable network support. We acknowledge support from the Ministry of Education, Culture, Sports, Science, and Technology (MEXT) of Japan, the Japan Society for the Promotion of Science (JSPS), and the Tau-Lepton Physics Research Center of Nagoya University; the Australian Research Council including Grants No. DP180102629, No. DP170102389, No. DP170102204, No. DP150103061, No. FT130100303; the Austrian Science Fund under Grant No. P 26794-N20; the National Natural Science Foundation of China under Contracts No. 11435013, No. 11475187, No. 11521505, No. 11575017, No. 11675166, No. 11705209; the Key Research Program of Frontier Sciences, Chinese Academy of Sciences (CAS), Grant No. QYZDJ-SSW-SLH011; the CAS Center for Excellence in Particle Physics (CCEPP); the Shanghai Pujiang Program under Grant No. 18PJ1401000; the Ministry of Education, Youth and Sports of the Czech Republic under Contract No. LTT17020; the Carl Zeiss Foundation, the Deutsche Forschungsgemeinschaft, the Excellence Cluster Universe, and the VolkswagenStiftung; the Department of Science and Technology of India; the Istituto Nazionale di Fisica Nucleare of Italy; the National Research Foundation (NRF) of Korea under Grants No. 2015H1A2A1033649, No. 2016R1D1A1B01010135, No. 2016K1A3A7A09005603, No. 2016R1D1A1B02012900, No. 2018R1A2B3003643, No. 2018R1A6A1A06024970, No. 2018R1D1A1B07047294; the Radiation Science Research Institute, Foreign Large-size Research Facility Application Supporting project, Global Science Experimental Data Hub Center of the Korea Institute of Science and Technology Information and KREONET/GLORIAD; the Polish Ministry of Science and Higher Education and the National Science Center; the Grant of the Russian Federation Government, Agreement No. 14.W03.31.0026; the Slovenian Research Agency; Ikerbasque, Basque Foundation for Science, Basque Government (Grant No. IT956-16) and Ministry of Economy and Competitiveness (MINECO) (Juan de la Cierva), Spain; the Swiss National Science Foundation; the Ministry of Education and the Ministry of Science and Technology of Taiwan; and the United States Department of Energy and the National Science Foundation.

[1] A. B. Carter and A. I. Sanda, *CP* violation in B meson decays, Phys. Rev. D **23**, 1567 (1981); I. I. Y. Bigi and A. I. Sanda, Notes on the observability of *CP* violations in B decays, Nucl. Phys. **B193**, 85 (1981).

[2] S. Faller, M. Jung, R. Fleischer, and T. Mannel, The golden modes $B^0 \to J/\psi K_{S,L}$ in the era of precision flavor physics, Phys. Rev. D **79**, 014030 (2009).

[3] M. Jung, Determining weak phases from $B \to J/\psi P$ decays, Phys. Rev. D **86**, 053008 (2012).

[4] K. De Bruyn and R. Fleischer, A roadmap to control penguin effects in $B_d^0 \to J/\psi K_S^0$ and $B_s^0 \to J/\psi\phi$, J. High Energy Phys. 03 (2015) 145.

[5] Z. Ligeti and D. J. Robinson, Towards More Precise Determinations of the Quark Mixing Phase β, Phys. Rev. Lett. **115**, 251801 (2015).

[6] M. Ciuchini, M. Pierini, and L. Silvestrini, The Effect of Penguins in the $B_d \to J/\psi K^0$ *CP* Asymmetry, Phys. Rev. Lett. **95**, 221804 (2005).

[7] P. Frings, U. Nierste, and M. Wiebusch, Penguin Contributions to *CP* Phases in $B_{d,s}$ Decays to Charmonium, Phys. Rev. Lett. **115**, 061802 (2015).

[8] S. E. Lee *et al.* (Belle Collaboration), Improved measurement of time-dependent *CP* violation in $B^0 \to J/\psi\pi^0$ decays, Phys. Rev. D **77**, 071101 (2008).

[9] B. Aubert *et al.* (*BABAR* Collaboration), Evidence for *CP* Violation in $B^0 \to J/\psi\pi^0$ Decays, Phys. Rev. Lett. **101**, 021801 (2008).

[10] K. Abe *et al.* (Belle Collaboration), Measurement of branching fractions and charge asymmetries for two-body B meson decays with charmonium, Phys. Rev. D **67**, 032003 (2003).

[11] A. Abashian *et al.* (Belle Collaboration), The Belle detector, Nucl. Instrum. Methods Phys. Res., Sect. A **479**, 117 (2002); also see the detector section in J. Brodzicka *et al.*, Physics achievements from the Belle experiment, Prog. Theor. Exp. Phys. **2012**, 4D001 (2012).

[12] D. J. Lange, The EvtGen particle decay simulation package, Nucl. Instrum. Methods Phys. Res., Sect. A **462**, 152 (2001).

[13] R. Brun *et al.*, GEANT 3.21, CERN Report No. DD/EE/84-1, 1984.

[14] P. Golonka and Z. Was, Photos Monte Carlo: A precision tool for QED corrections in Z and W decays, Eur. Phys. J. C **45**, 97 (2006).

[15] M. Tanabashi *et al.* (Particle Data Group), Review of particle physics, Phys. Rev. D **98**, 030001 (2018).

[16] G. C. Fox and S. Wolfram, Observables for the Analysis of Event Shapes in e^+e^- Annihilation and Other Processes, Phys. Rev. Lett. **41**, 1581 (1978).

[17] H. Kakuno *et al.* (Belle Collaboration), Neutral B flavor tagging for the measurement of mixing induced *CP* violation at Belle, Nucl. Instrum. Methods Phys. Res., Sect. A **533**, 516 (2004).

[18] K. Abe *et al.* (Belle Collaboration), Improved measurement of *CP*-violation parameters $\sin 2\phi_1$ and $|\lambda|$, B meson lifetimes, and $B^0 - \bar{B}^0$ mixing parameter Δm_d, Phys. Rev. D **71**, 072003 (2005); Erratum **71**, 079903 (2005).

[19] I. Adachi *et al.* (Belle Collaboration), Precise Measurement of the *CP* Violation Parameter $\sin 2\phi_1$ in $B^0 \to (c\bar{c})K^0$ Decays, Phys. Rev. Lett. **108**, 171802 (2012).

[20] T. Skwarnicki, A study of the radiative cascade transitions between the Upsilon-prime and Upsilon resonances, Deutsches Elektronen-Synchrotron (DESY) Report No. DESY-F31-86-02.

[21] K. S. Cranmer, Kernel estimation in high energy physics, Comput. Phys. Commun. **136**, 198 (2001).

[22] H. Albrecht *et al.* (ARGUS Collaboration), Search for hadronic $b \to u$ decays, Phys. Lett. B **241**, 278 (1990).

[23] S. Ryu *et al.* (Belle Collaboration), Measurements of branching fractions of τ lepton decays with one or more K_S^0, Phys. Rev. D **89**, 072009 (2014).

[24] Y. Amhis *et al.* (Heavy Flavor Averaging Group Collaboration), Averages of b-hadron, c-hadron, and τ-lepton properties as of summer 2016, Eur. Phys. J. C **77**, 895 (2017).

[25] O. Long, M. Baak, R. N. Cahn, and D. P. Kirkby, Impact of tag side interference on time dependent *CP* asymmetry measurements using coherent $B^0\,\bar{B}^0$ pairs, Phys. Rev. D **68**, 034010 (2003).

[26] P. Avery *et al.* (CLEO Collaboration), Study of exclusive two-body B^0 meson decays to charmonium, Phys. Rev. D **62**, 051101 (2000).